Optimal Sensing Geometry for Pseudorange and Bearing-Elevation Observations

Jonghyuk Kim and Weikun Chen
The Australian National University, Australia
{jonghyuk.kim, wayne.chen}@anu.edu.au

Abstract

In this paper, we investigate the sensing geometry in the context of tightly-coupled simultaneous localisation and mapping, which fuses pseudoranges from GPS satellites and the bearing-elevation observations from ground landmarks. The concept of geometrical dilution of precision has been widely applied for the pseudorange observations but needs to be generalised to account for the angular measurements. In this work, we derive a closed-form solution for the determinant of the Fisher information matrix using a minimal set of observations, which offers insights on the optimal sensing geometry and thus the effective sensing strategy.

1 INTRODUCTION

The geometry of sensors-to-beacons/targets can significantly affect the performance of navigation or target-tracking systems and has been extensively investigated in integrated navigation, target-tracking and sensor network communities leading to the concept of geometrical dilution of precision (GDOP) [Langley, 1999][Bishop *et al.*, 2010].

For example, most GPS receivers provide GDOP information to the users which, in essence, captures the amplification of pseudorange errors to navigational (both positioning and timing) errors [Langley, 1999]. This GDOP concept has been studied in the sensor network and target localisation to identify the optimal sensor-target configurations. In [Bishop *et al.*, 2010], the optimal sensor-to-target geometries were characterised for bearing-only, range-only or angle-of-arrival sensors. The fundamental idea is that such geometrical configurations are likely to improve the localisation accuracy.

In active simultaneous localisation and mapping (SLAM), there has been extensive work on selecting the informative features utilising the information theory [Bryson and Sukkarieh, 2008][Leung *et al.*, 2008][H. Strasdat and Burgard., 2009][Cadena *et al.*, 2016]. [Bryson and Sukkarieh, 2008] utilised the entropic information gain to quantify the amount of average information expected from the sensors, which is then used for the vehicle guidance. [Leung *et al.*, 2008] used the entropic information gain for the exploration and motion planning to minimise the uncertainty of SLAM system.

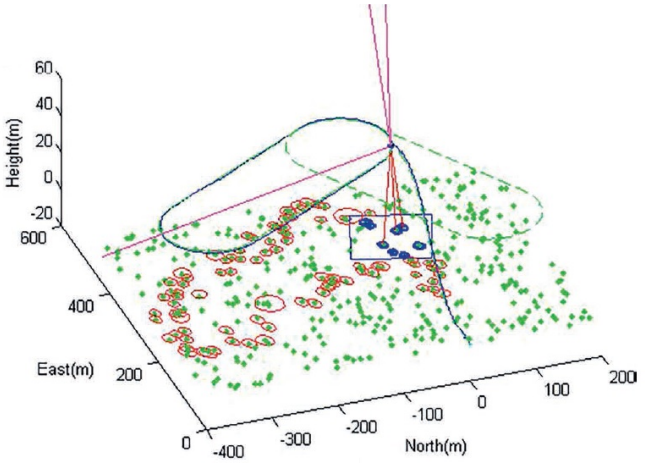

Figure 1: A sensing scenario used in this work showing GPS pseudoranges (3 skywards rays) and visual bearing/elevations (3 down-looking rays). The diagram shows an aerial SLAM simulation with with estimated landmark positions and uncertainties (blue - active map; red - inactive map; green - true map).

Although these developments have managed to understand the geometrical effects of individual sensing modality, there has been limited work for the heterogeneous sensing system or the closed-form expression of the information gain for a vehicle operating in a fully 3D environment. In this work, we consider a tightly-integrated navigation system which fuses GPS pseudoranges, bearing and elevation information. Figure 1 illustrates the sensing scenario for an aerial vehicle application, showing three skywards rays to the GPS satellites and three downwards rays to the landmark features on the ground

Figure 2: An example of aerial down-looking camera outputs. Features detected are represented in pixel coordinates (u, v) and are converted to bearing and elevation (ϕ, θ) to be fused in the navigation system.

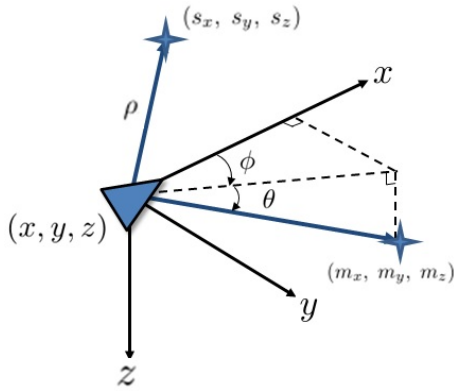

Figure 3: The sensing diagram for pseudorange (ρ), bearing (ϕ) and elevation (θ) observations. All the satellite and landmark positions are expressed in a body-coordinate system: x(roll), y(pitch) and z(yaw). (s_x, s_y, s_z) and (m_x, m_y, m_z) are the satellite and landmark position, respectively.

[Kim *et al.*, 2017]. In our previous work [Kim *et al.*, 2016], a preliminary analysis was performed on the bearing and elevations and their geometrical effects on the navigational performance. This work will further analyse the sensing geometry as well as proposing an optimal sensing strategy. The contribution of this work is twofold:

- Closed-form expressions of the optimal sensing geometry using a minimal set of pseudorange, bearing and elevation
- Optimal landmark sensing strategies to complement the weak horizontal or vertical navigational performance.

Understanding the optimal sensing configuration given a fixed number of satellites and landmarks can be effectively used a trade-off between the computational complexity and the navigational accuracy.

The outline of this work is as follows: Section 2 will briefly discuss on how the bearing and elevation angles are computed from the camera pixel measurements and Section 3 will provide the nonlinear and linearised observation models used in this work. Section 4 will evaluate the Fisher information matrix for a minimal set of observations and derive closed-form solutions for the determinant of the Fisher information matrix. Section 5 proposes practical sensing strategies to improve the navigational accuracy either in horizontal or vertical direction, followed by Conclusion future work.

2 Image Features to Bearing and Elevation

Figure 2 depicts an example of aerial camera images [Kim and Sukkarieh, 2007]. Any detected visual features are expressed in the (u, v) pixel coordinates system and need to be converted to the bearing-elevation obsevations (ϕ^c, θ^c) in the camera frame as

$$\phi^c = \arctan \frac{(u - u_0)}{f_u} \tag{1}$$

$$\theta^c = \arctan \left[\tan \frac{(v - v_0)}{f_v} \cos \phi^c \right], \tag{2}$$

with (u_0, v_0) being the camera centre and (f_u, f_v) the focal length. To be processed in the navigation system, the (ϕ^c, θ^c) are further converted to the bearing-elevation (ϕ, θ) expressed in the body-coordinate frame by applying the 90° rotation along the pitch axis.

3 Observation Models

A body-coordinate frame and observations are illustrated in Figure 3 with a satellite position of $[s_x,\ s_y,\ s_z]^T$ and a landmark position of $[m_x,\ m_y,\ m_z]^T$. The satellite position can be predicted accurately from the ephemeris data periodically available from the satellite, and the landmark locations are initialised using the triangulation method during the initial mapping stage. The nonlinear observation model for the pseudorange (ρ), bearing (ϕ) and elevation (θ), and the navigational state consisting of the vehicle position (x, y, z) and the clock bias $(c\Delta t)$ is

$$\mathbf{z} = h(\mathbf{x}) + \mathbf{v}, \tag{3}$$

which consists of

$$\rho_i = \sqrt{(s_x^i - x)^2 + (s_y^i - y)^2 + (s_z^i - z)^2} + c\Delta t + v_\rho$$

$$\phi_i = \arctan \frac{(m_y^i - y)}{(m_x^i - x)} + v_\phi$$

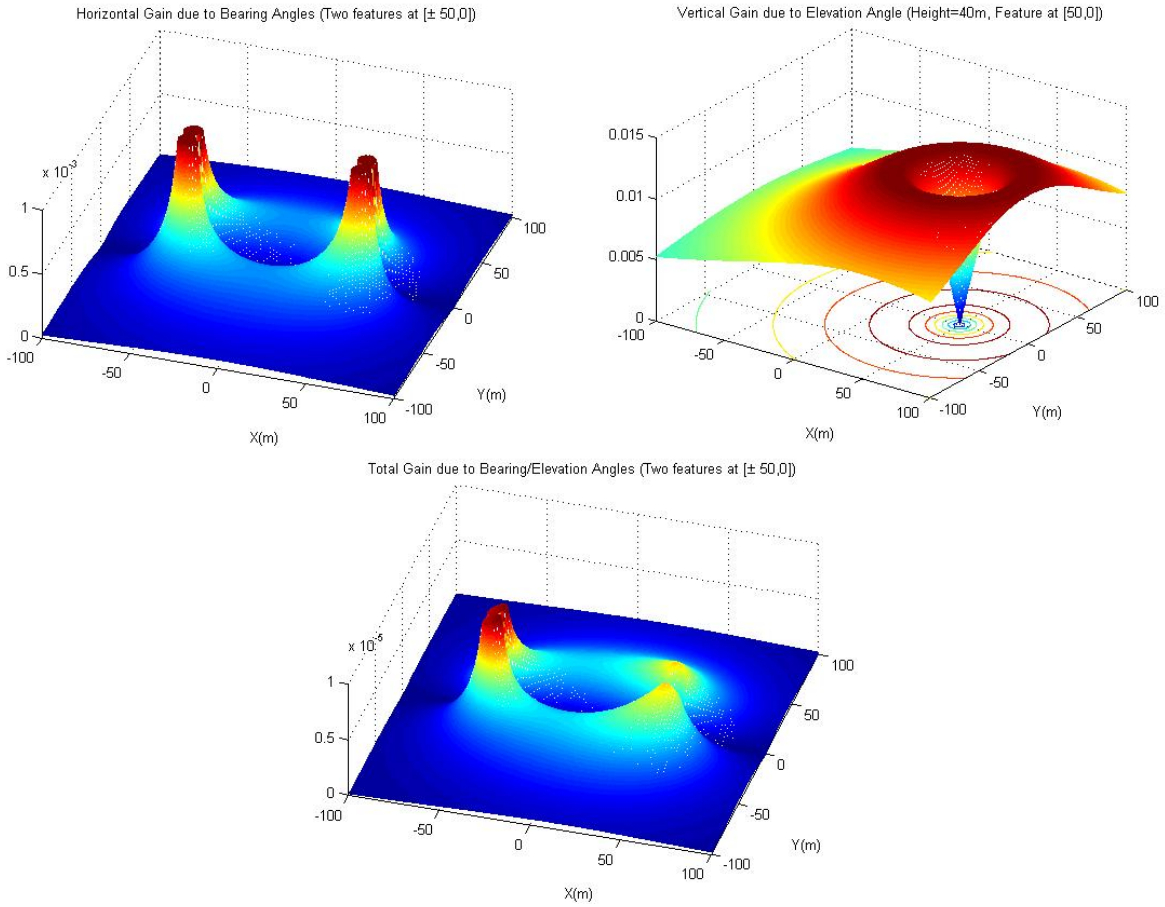

Figure 4: The information gain for the Case-1: (Top left) the horizontal information gain due to two bearing observations. (Top right) the vertical contribugain tion from a single elevation observation. (Bottom) the combined total information gain. In this analysis, two landmarks are located at $(\pm 50, 0, 0)$ and the vehicle has a constant height of 40m. Note the the zero-gain effect of the 90° elevation on the vertical information gain.

$$\theta_i = \arctan \frac{(m_z^i - z)}{\sqrt{(m_x^i - x)^2 + (m_y^i - y)^2}} + v_\theta$$

where $(v_\rho, v_\phi, v_\theta)$ are the sensing noises with zero-means and strengths of $(\sigma_\rho^2, \sigma_\phi^2, \sigma_\theta^2)$.

The linearised observation model can be obtained by computing Jacobians, giving

$$\mathbf{z} = \mathbf{H}\mathbf{x} + \mathbf{v}, \tag{4}$$

with

$$\mathbf{H}_{\rho i} = \left[\frac{-(s_x^i - x)}{r_i}, \frac{-(s_x^i - x)}{r_i}, \frac{-(s_z^i - z)}{r_i}, 1\right] \tag{5}$$

$$\mathbf{H}_{\phi i} = \left[\frac{\sin\phi_i}{r_{hi}}, \frac{-\cos\phi_i}{r_{hi}}, 0, 0\right] \tag{6}$$

$$\mathbf{H}_{\theta i} = \left[\frac{\cos\phi_i \sin\theta_i}{r_i}, \frac{\sin\phi_i \sin\theta_i}{r_i}, \frac{-\cos\theta_i}{r_i}, 0\right] \tag{7}$$

where r_i is the true range to either i^{th} satellite or i^{th} landmark, and r_{hi} is the horizontal range to the i^{th} landmark: $\sqrt{(m_x^i - x)^2 + (m_y^i - y)^2}$.

4 Fisher Information Matrix and Information Measure

The fundamental question is, given a set of satellite and landmarks, what sensing geometry would provide maximal information (or minimal uncertainty) to the navigational state?

To address this question, we utilise the Fisher information matrix rather than the conventional covariance matrix as used in GPS systems. The information space formulation provides the benefit of additive property of the information — that is, the total information is simply the summation of individual information gained from each sensor. Therefore the total information for the sys-

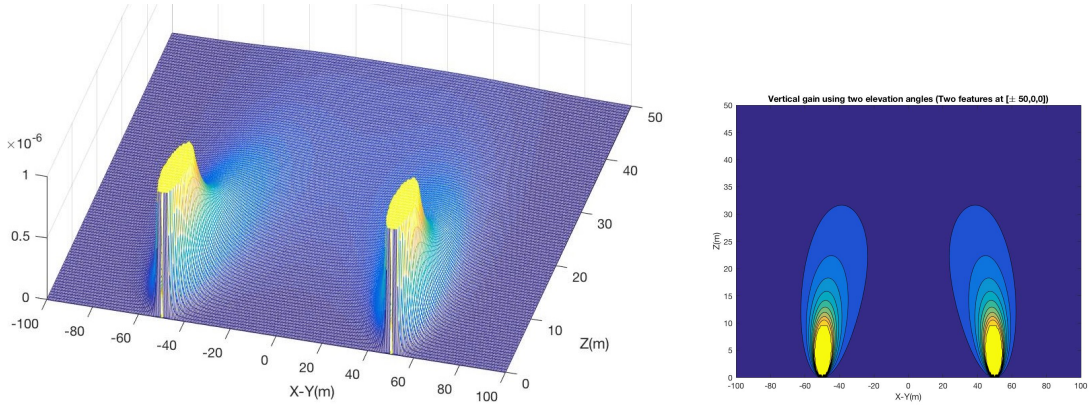

Figure 5: The height information gain for the Case-2 using two elevation angles; 3D plot (left) and 2D plot (right). The figures show the vertical section of the sensing geometry assuming the vehicle follows a straight line connecting two landmarks located at $[\pm 50, 00]$. It can be seen that the height informatin increases as the vehicle flies closes to the landmarks as well as maintaing the relative eleavation angle as 90°.

tem in Equation 4 becomes

$$\mathbf{I} \triangleq \sum \mathbf{H}^T \mathbf{R}^{-1} \mathbf{H} \tag{8}$$

$$= \frac{1}{\sigma_\rho^2} \sum_{i=1}^{N_s} \mathbf{H}_{\rho i}^T \mathbf{H}_{\rho i} + \frac{1}{\sigma_\phi^2} \sum_{i=1}^{N_m} \mathbf{H}_{\phi i}^T \mathbf{H}_{\phi i} + \frac{1}{\sigma_\theta^2} \sum_{i=1}^{N_m} \mathbf{H}_{\theta i}^T \mathbf{H}_{\theta i} \tag{9}$$

where N_s and N_m are the total number of observed satellite vehicles and landmarks, respectively.

As an information metric to quantify the amount of information, a trace or a determinant of the information matrix is typically used. The trace is the summation of the eigenvalues and thus captures the average certainty to each direction, although dominated by the largest eigenvalue. On the other hand, the determinant is the product of the eigenvalues and thus expresses the volume of the total information which is affected by both the largest and smallest eigenvalues. Traditional GPS systems utilise the trace of the covariance matrix, and thus the GDOP metric captures the average uncertainty. In information space, the trace is also related to the Cramer-Rao lower Bound (CRB) which an efficient unbiased estimator can achieve,

$$\mathrm{tr}(\mathbf{I}) = \mathrm{tr}\left(\sum \mathbf{H}^T \mathbf{R}^{-1} \mathbf{H}\right) \tag{10}$$

$$= \frac{2N_s}{\sigma_\rho^2} + \frac{1}{\sigma_\phi^2} \sum_{i=1}^{N_m} \frac{1}{r_{hi}^2} + \frac{1}{\sigma_\theta^2} \sum_{i=1}^{N_m} \frac{1}{r_i^2} \tag{11}$$

$$\triangleq \mathrm{CRB}^{-1}. \tag{12}$$

The determinant of the information matrix in Equation 8 can also be evaluated for each sensing modality with some conditions as in [Bishop 07]. Note that individual information contribution matrix has a rank of one, and thus the determinant becomes zero, requiring a collection of enough number of observations. To gain further insight into the heterogeneous sensing system, we consider a minimal set of observations — as there are 4 unknowns x, y, z and $c\Delta t$, 4 observations are required. Therefore we consider two cases consisting of 4 pieces of information,

- Case 1: $\boldsymbol{z} = [\phi_1,\ \phi_2,\ \theta_1,\ \rho_1]^T$
- Case 2: $\boldsymbol{z} = [\phi_1,\ \theta_1,\ \theta_2,\ \rho_1]^T$.

Note that from Equations 5-7, it can be observed that a bearing observation does not provide any information on the height and the clock bias, nor an elevation observation on the clock bias.

4.1 The determinant for the Case-1

For the Case 1, the combined observation matrix becomes

$$\mathbf{H} = \begin{bmatrix} \frac{\sin\phi_1}{r_{h1}} & \frac{-\cos\phi_1}{r_{h1}} & 0 & 0 \\ \frac{\sin\phi_2}{r_{h2}} & \frac{-\cos\phi_2}{r_{h2}} & 0 & 0 \\ \frac{\cos\phi_1 \sin\theta_1}{r_1} & \frac{\sin\phi_1 \sin\theta_1}{r_1} & \frac{-\cos\theta_1}{r_1} & 0 \\ \frac{-(s_x^1 - x)}{r_1^s} & \frac{-(s_x^1 - x)}{r_1^s} & \frac{-(s_z^1 - z)}{r_1^s} & 1 \end{bmatrix}. \tag{13}$$

As the matrix is a square-matrix, the determinant of the information matrix becomes

$$\det(\mathbf{I}) = \det\left(\mathbf{H}^T \mathbf{R}^{-1} \mathbf{H}\right) = \frac{1}{\sigma_\phi^4 \sigma_\theta^2 \sigma_\rho^2} \det\left(\mathbf{H}\right)^2 \tag{14}$$

The $\det\left(\mathbf{H}\right)^2$ is purely a geometrical factor and can be found from Equation 13 by inspection, yielding

$$\det\left(\mathbf{H}\right)^2 = \underbrace{\frac{\sin^2(\phi_1 - \phi_2)}{r_{h1}^2 r_{h2}^2}}_{x-y} \times \underbrace{\frac{\cos^2\theta_1}{r_1^2}}_{z} \times \underbrace{\frac{1}{t}}. \tag{15}$$

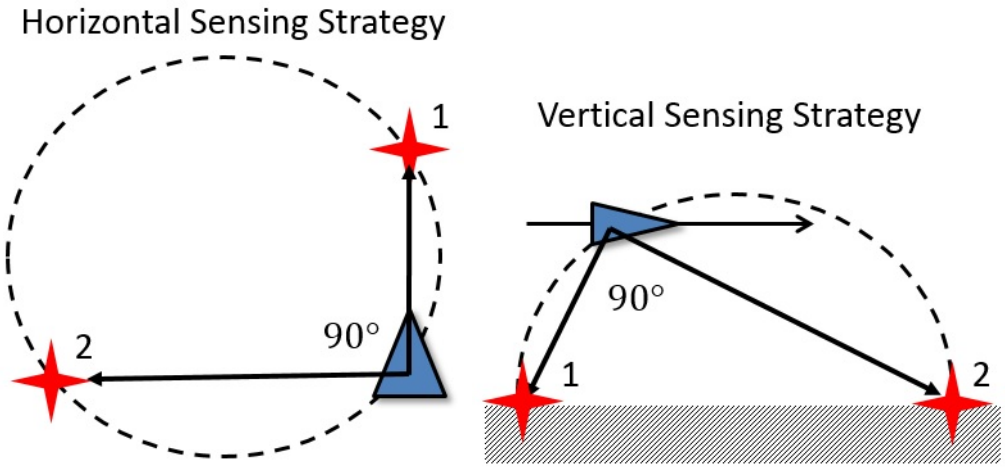

Figure 6: An optimal sensing strategy to improve the horizontal accuracy using two bearing observations (left) and an optimal strategy to improve the vertical accuracy using two elevation observations (right).

From this closed-form expression, it can be observed that

- The two bearing observations from two landmarks contribute to the horizontal information gain, which has two poles at $r_{h1} = 0$ and $r_{h2} = 0$, and a maximum local gain along the circumference. which satisfies the constraint of $\phi_{12} = \pm 90°$.
- The single elevation observation from a landmark contributes to the height information gain, which has a maximum value when $\theta_1 = \pm 45°$ (proof is omitted here but utilises $r_1 = h_0 \csc \theta_1$.)
- The single pseudorange observation contributes to the clock bias information in an isotropic way (thus not affected by the sensing direction).

These results correspond to the fact that two bearing rays intersecting at 90° have a minimal uncertainty volume given fixed ranges. Figure 4 depicts the determinant of the information for the Case-1, showing the information gain from two-bearings, an elevation, and the combined information. Note the zero-gain effect of the 90° elevation angle, lowering the total information gain around the landmark 1. This is because the cone formed by 90° elevation observation degenerates to a line and thus does not provide any information on the height

4.2 The determinant for the Case-2

For the Case 2, the combined observation matrix becomes

$$\mathbf{H} = \begin{bmatrix} \frac{\sin\phi_1}{r_{h1}} & \frac{-\cos\phi_1}{r_{h1}} & 0 & 0 \\ \frac{\cos\phi_1 \sin\theta_1}{r_1} & \frac{\sin\phi_1 \sin\theta_1}{r_1} & \frac{-\cos\theta_1}{r_1} & 0 \\ \frac{\cos\phi_2 \sin\theta_2}{r_2} & \frac{\sin\phi_2 \sin\theta_2}{r_2} & \frac{-\cos\theta_2}{r_2} & 0 \\ \frac{-(s_x^1 - x)}{r_1^s} & \frac{-(s_x^1 - x)}{r_1^s} & \frac{-(s_z^1 - z)}{r_1^s} & 1 \end{bmatrix}. \quad (16)$$

The determinant becomes a bit more complicated but can be expressed in closed-form as

$$\det(\mathbf{H})^2 = \left[\frac{\sin\theta_1 \cos\theta_2 - \cos\theta_1 \sin\theta_2 (\cos(\phi_1 - \phi_2))}{r_1 r_2 r_{h1}} \right]^2. \quad (17)$$

If we consider a case when the two landmarks and the vehicle are aligned along a line, then $\phi_1 = \phi_2$ or $\phi_1 = \phi_2 \pm \pi$, simplifying the result as

$$\det(\mathbf{H})^2 = \underbrace{\frac{1}{r_{h1}^2}}_{x-y} \times \underbrace{\frac{\sin^2(\theta_1 - \theta_2)}{r_1^2 r_2^2}}_{z} \times \underbrace{1}_{t}. \quad (18)$$

This implies that

- The single bearing observation contributes to the horizontal information in an isotropic way.
- The two elevation views contribute to the height information gain, with $\theta_{ij} = \pm 90°$ maximising the sine term. This is because two elevation cones intersecting at 90° have a minimal uncertainty volume given fixed ranges.
- The single pseudorange observation contributes to the clock time information in an isotropic way.

These are illustrated in Figure 5 showing the determinant with two elevation angles. The figures show the vertical section of the sensing geometry assuming the vehicle follows a straight line connecting two landmarks located at $[\pm 50, 00]$. It can be seen that the height informatin increases as the vehicle flies closes to the landmarks as well as maintaing the relative eleavation angle as 90°.

5 Optimal Sensing Strategy

Based on these results, we propose practical sensing strategies for a minimal set of observations consisting of two landmarks and one satellite vehicle. In particular, when the navigational system shows poor performance either in horizontal or vertical direction, certain landmarks sensing configuration can complement the performance. Figure 6 (left) illustrates a sensing configuration for two landmarks when the navigational system exhibits reduced horizontal accuracy. The landmark selection procedures are

1. Select the *cloest* landmark 1, for example along the heading direction, as the horizontal gain increases inversely proportional to the squared distance.
2. Select the second landmark 2 which has a $\pm 90^\circ$ relative bearing angle with respect to the first landmark.
3. If possible, follow the circumference trajectory formed by the two landmarks to maximise the horizontal information gain.

Another case is when the navigational system shows reduced vertical performance, and two landmarks can be selected as shown in Figure 6 (right). Assuming the landmarks and vehicle are along a straight line,

1. Select the landmark 1 with 45° or 135° elevation angle which can maximise the vertical gain.
2. Select the second landmark 2 which has a 90° relative elevation angle with respect to the first landmark.
3. If possible, follow the upper-circumference trajectory to maximise the vertical information gain.

In summary, the information gain can be maximised if the vehicle navigates as closely as possible to the landmarks while maintaining the 90° relative bearing or elevation angle. This matches the physical intuition that two visual ray observations form the smallest uncertainty volume when they intersect at 90° given fixed ranges.

6 Conclusions

Extending the concept of GDOP widely used in GPS systems, this work analysed the optimal sensing geometry for GPS pseudoranges, camera-bearing and elevation observations in a tightly-integrated navigation system. The work utilises the Fisher information matrix from the linearised observation models, and the determinant of the Fisher information matrix was evaluated as an information gain metric. For a minimal set of observations, closed-form solutions of the information gain were derived for two sensing scenarios. The main findings are 1) the horizontal information gain can be maximised by taking 90° relative bearing angles from the closest landmarks, and 2) the vertical information gain can be maximised by taking 90° relative elevation angle from the closest landmarks. Two optimal sensing strategies were then proposed for the vehicle to follow the surface of the cylinder or hemisphere formed by the two landmarks. Future work includes extending the results for the case of N-number of landmark observations.

References

[Bishop *et al.*, 2010] Adrian N. Bishop, Bars Fidan, Brian D. O. Anderson, Kutluyl Dogancay, and Pubudu N. Pathirana. Optimality analysis of sensor-target localization geometries. *Automatica*, 46(3):479–492, March 2010.

[Bryson and Sukkarieh, 2008] Mitch Bryson and Salah Sukkarieh. Observability analysis and active control for airborne slam. *IEEE Transactions on Aerospace and Electronic Systems*, 44(1), 2008.

[Cadena *et al.*, 2016] C. Cadena, L. Carlone, H. Carrillo, Y. Latif, D. Scaramuzza, J. Neira, I. Reid, and J.J Leonard. Past, present, and future of simultaneous localization and mapping: Toward the robust-perception age. *IEEE Transactions on Robotics*, 32(6):1309–1332, 2016.

[H. Strasdat and Burgard., 2009] C. Stachniss H. Strasdat and W. Burgard. "which landmark is useful? learning selection policies for navigation in unknown environments. In *IEEE International Conference on Robotics and Automation*, pages 1410–1415, Kobe, 2009.

[Kim and Sukkarieh, 2007] Jonghyuk Kim and Salah Sukkarieh. Real-time implementation of airborne inertial-slam. *Robotics and Autonomous Systems*, 55(1):62–71, Jan. 2007.

[Kim *et al.*, 2016] J. Kim, J. Cheng, and J. Guivant. Tightly-coupled integration of gps/ins and simultaneous localisation and mapping. In *Australasian Conference on Robotics and Automation*, Brisbane, 2016.

[Kim *et al.*, 2017] J. Kim, J. Cheng, J. Guivant, and J. Nieto. Compressed fusion of gnss/inertial navigation and simultaneous localization and mapping. *IEEE Aerospace and Electronic Systems Magazine*, August 2017.

[Langley, 1999] R. B. Langley. Dilution of precision. *GPS World*, May 1999.

[Leung *et al.*, 2008] C. Leung, Shoudong Huang, and G. Dissanayake. Active slam in structured environments. In *2008 IEEE International Conference on Robotics and Automation*, pages 1898–1903, May 2008.